THE JOURNAL OF PHYSICAL CHEMISTRY B

Article

pubs.acs.org/JPCB

Effects of Electronic-State-Dependent Solute Polarizability: Application to Solute-Pump/Solvent-Probe Spectra

Xiang Sun,[†] Branka M. Ladanyi,*[,‡] and Richard M. Stratt*[,†]

[†]Department of Chemistry, Brown University, Providence, Rhode Island 02912, United States

[‡]Department of Chemistry, Colorado State University, Fort Collins, Colorado 80523-1872, United States

Supporting Information

ABSTRACT: Experimental studies of solvation dynamics in liquids invariably ask how changing a solute from its electronic ground state to an electronically excited state affects a solution's dynamics. With traditional time-dependent-fluorescence experiments, that means looking for the dynamical consequences of the concomitant change in solute−solvent potential energy. But if one follows the shift in the dynamics through its effects on the macroscopic polarizability, as recent solute-pump/solvent-probe spectra do, there is another effect of the electronic excitation that should be considered: the jump in the solute's own polarizability. We examine the spectroscopic consequences of this solute polarizability change in the classic example of the solvation dye coumarin 153 dissolved in acetonitrile. After demonstrating that standard quantum chemical methods can be used to construct accurate multisite models for the polarizabilities of ground- and excited-state solvation dyes, we show via simulation that this polarizability change acts as a contrast agent, significantly enhancing the observable differences in optical-Kerr spectra between ground- and excited-state solutions. A comparison of our results with experimental solute-pump/solvent-probe spectra supports our interpretation and modeling of this spectroscopy. We predict, in particular, that solute-pump/solvent-probe spectra should be sensitive to changes in both the solvent dynamics near the solute and the electronic-state-dependence of the solute's own rotational dynamics.

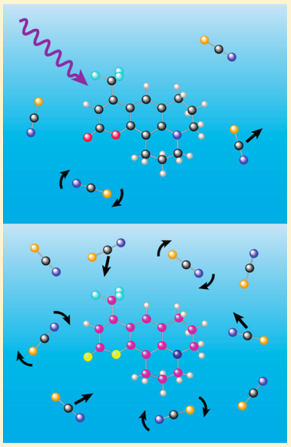

I. INTRODUCTION

One of the more intriguing developments in the ongoing attempt to devise progressively more revealing probes of dynamics in liquids is the introduction of an interesting class of solute-pump/solvent-probe spectroscopies.[1−13] Rather than using light scattering to measure the polarizability fluctuations (and thus the intermolecular vibrational dynamics) of the liquid as a whole—as optical-Kerr-effect (OKE) spectroscopies do[14,15]—or trying to infer what is happening in the liquid by watching a solute's fluorescence red shift following its own electronic excitation (the strategy of time-dependent-fluorescence studies),[16] these solute-pump/solvent-probe methods look at how the intermolecular vibrational spectroscopy of an entire solution is affected by the electronic excitation of a solute. That means that they can watch how the rapid solution librational and translational dynamics evolves as the solvation process gradually remakes the solvent structure.[13]

Experimental realizations of such spectra are now starting to appear,[1−4,6−11] as are theoretical analyses of what these spectra can tell us.[5,12,13] In one such experiment, the Scherer group[6,7] used resonant-pump polarizability response spectroscopy (RP-PORS) to revisit the dynamics of one of the most classic solvation examples, coumarin 153 dissolved in acetonitrile.[17−19] By carrying out transient-grating spectroscopy as a function of the time delay since excitation of the coumarin, they were able to measure how the solution's rapid polarizability fluctuations (reported on a time scale t) changed with the structural-relaxation time T, providing them with a genuine two-dimensional (t, T) portrait of the whole solvation process.

The parallel theoretical studies have shown that such two-dimensional (2-d) spectra are intertwinings of polarizability-fluctuation and structural-relaxation dynamics rather than two completely separable pieces.[5,12,13] Nonetheless the full 2-d spectrum has been calculated for a model atomic liquid mixture exhibiting preferential solvation,[13] a phenomenon whose very existence stems from the ability of a mixture to undergo significant structural reorganization on solute excitation.[20−23] The results in this example make clear that this spectroscopy is well-suited to extracting both the relaxation dynamics of solute−solvent interaction energies (the province of traditional time-dependent-fluorescence studies) and the solvation shell population dynamics (an explicitly structural component of the dynamics)—and that both pieces are needed to understand how solvation happens.[13]

Interestingly, though, it is not entirely obvious why one can even see a signal from this experiment. In the limit at which the observed structural-relaxation time T is large enough, these spectra simply report the difference between the OKE spectrum

Special Issue: Branka M. Ladanyi Festschrift

Received: September 5, 2014
Revised: October 8, 2014
Published: October 9, 2014

   dx.doi.org/10.1021/jp509021c | J. Phys. Chem. B 2015, 119, 9129−9139

of the solution with an excited-state solute and that with a ground-state solute.[12] But in a typical dilute solution there are many more solvent molecules largely unaffected by solutes than there are ones that are strongly perturbed—so why should one be able to see an excited-state/ground-state shift in the solvent polarizability dynamics against the large backdrop of solute-indifferent solvent polarizability dynamics?

Part of the answer is that the large dye molecules often used as solutes in solvation experiments have the largest polarizabilities in the system.[24] In our atomic mixture study,[12,13] this feature amplified the solute−solvent interaction-induced portion of the many-body polarizability $\mathbf{\Pi}$,[25] and therefore highlighted the solvation-related dynamics. But in systems such as coumarin 153 (C153) in acetonitrile, the purely molecular, noninteraction-induced, contributions dominate acetonitrile's $\mathbf{\Pi}$.[26−28] There must be something else that helps in such cases.

In this work, we suggest that the key feature is something that had been left out of previous theoretical studies: the often significant change in solute polarizability on electronic excitation. As we show by looking explicitly at the simulated solute-pump/solvent-probe spectra of C153 in acetonitrile, the ground-state → excited-state change in the C153 polarizability is precisely what makes the dynamics in the vicinity of the solute visible; omitting that change effectively zeroes out the signal.

The remainder of this work will be organized as follows: Section II will present our basic model for the solvation dynamics of this solution and for its OKE spectroscopy. A realistic treatment requires a many-site model of the coumarin's interaction with the acetonitrile solvent,[29,30] along with distributed (multisite) representations of the polarizability tensors of both solution components.[27,31−35] However, all of these requirements have previously been dealt with in the literature. The new technical development, though, is in section III, where we show that routine quantum chemistry methods used with standard basis sets can provide us with accurate polarizability tensors for both the ground and first-excited states of molecules with features typical of solvation dyes. We then show that the site charges derived from the quantum chemistry calculations supply us with enough of a guide that we can fit these ground- and excited-state polarizability tensors to the multisite polarizability models needed for solution simulations. In section IV, we make use of these results to compute the (large-T limit of the) solute-pump/solvent-probe spectrum and analyze the principal contributions to the spectrum. Finally in section V, we conclude with some general remarks.

II. BASIC MODEL

A. Component Molecules and Their Interactions. Our C153 in acetonitrile solution is built largely (though not entirely) out of the same ingredients employed in the earlier study of solvation dynamics by Ingrosso et al.[30] The system considered here consists of a single, rigid, all-atom (36-site) coumarin 153 ($C_{16}H_{14}F_3NO_2$) molecule (Figure 1) and 244 rigid 3-site acetonitrile (Me—C≡N) molecules.

All of the intermolecular interactions between sites a on one molecule and b on another are sums of Lennard-Jones plus Coulombic terms

$$u_{ab}(r_{ab}) = 4\varepsilon_{ab}\left[\left(\frac{\sigma_{ab}}{r_{ab}}\right)^{12} - \left(\frac{\sigma_{ab}}{r_{ab}}\right)^{6}\right] + \frac{q_a q_b}{(4\pi\varepsilon_0)r_{ab}} \tag{2.1}$$

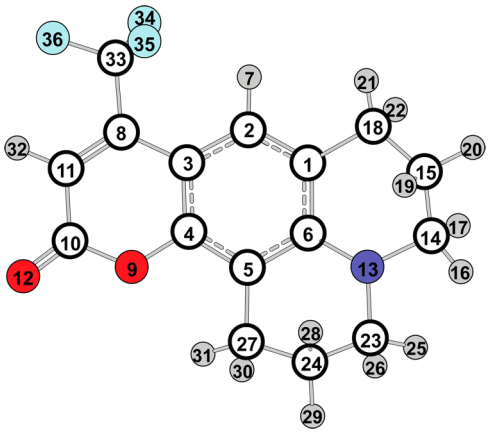

Figure 1. Coumarin 153 (C153) showing the atom numbering system we use in this work. Open circles are C atoms, small gray circles are H atoms, atom 13 is N, atoms 9 and 12 are O, and atoms 34−36 are F.

with r_{ab} being the distance between the sites and the quantities σ, ε, and q site-specific parameters. The site−site Lennard-Jones parameters σ_{ab} and ε_{ab}, in particular, are calculated from the optimized potentials for liquid simulations (OPLS) combining rules[36]

$$\sigma_{ab} = \sqrt{\sigma_a\sigma_b}, \qquad \varepsilon_{ab} = \sqrt{\varepsilon_a\varepsilon_b} \tag{2.2}$$

from the individual σ and ε site values and are assumed to be identical for ground- and excited-state C153 molecules.

All of the parameters of the acetonitrile molecules (the site−site intramolecular distances as well as the Lennard-Jones parameters and charges q for the individual sites) are taken from Gee and van Gunsteren's empirical model.[37] Lennard-Jones parameters for the coumarin come from standard literature OPLS values,[36,38] but the remaining details for C153, the molecular geometry and the different ground-state and first-electronic-excited-state values for the site charges, are derived by Ingrosso et al.[30] from quantum chemical calculations incorporating the acetonitrile solvent at the level of a polarizable continuum (a step needed in order to produce realistic solution-phase dipole moments and partial charges). That work also considered the effects of flexible intramolecular geometries and excited-state/ground-state geometry changes, but we confine ourselves here to C153 solutes with geometries fixed at the ground-state-optimized values since the intramolecular structure does not changes much on electronic excitation.[30] The complete set of acetonitrile and C153 geometries and interaction parameters we use is tabulated in the Supporting Information for this work.

B. Many-Body and Molecular Polarizabilities. Since the signal in a four-wave mixing experiment (such as optical-Kerr or transient-grating spectroscopy)[39] is a direct reflection of the dynamics of the many-body polarizability tensor, $\mathbf{\Pi}(t)$, it is also of some importance to have a representative model for that polarizability. Molecular polarizabilities, in particular, are best thought of as arising from multiple sites within each molecule.[31−34] Accordingly, in a solution with a total of M sites, the 3 × 3 polarizability tensor for the solution as a whole, $\mathbf{\Pi}$, can be written as a sum over all of the liquid-phase individual-site polarizability tensors $\boldsymbol{\pi}_j$, each of which, in turn, can be written as a sum of contributions from the corresponding isolated-site's polarizability, $\boldsymbol{\alpha}_j$, and the interaction-induced contributions from the other sites.[25]

dx.doi.org/10.1021/jp509021c | J. Phys. Chem. B 2015, 119, 9129−9139

$$\boldsymbol{\Pi} = \sum_{j=1}^{M} \boldsymbol{\pi}_j \tag{2.3}$$

$$\boldsymbol{\pi}_j = \boldsymbol{\alpha}_j + \sum_{k\neq j}^{M} \boldsymbol{\alpha}_j \cdot \mathbf{T}_{jk} \cdot \boldsymbol{\pi}_k \tag{2.4}$$

The induced-dipole/induced-dipole interaction tensor $\mathbf{T}_{jk}$, which acts between sites j and k, has to revert to its well-known point-dipole/point-dipole form in the limit of large site−site distances, but that form is unphysical at the shortest distances encountered in liquids. We thus make use of the exponential Thole version of this tensor, a model form designed to interpolate correctly between the requisite distance limits.[31]

$$\begin{aligned} \mathbf{T}_{jk} &= [(3f^T(x)\,\hat{\mathbf{r}}\hat{\mathbf{r}} - f^E(x)\,\mathbf{1})/r^3]_{\mathbf{r}=\mathbf{r}_{jk}, x=ar_{jk}/(\alpha_j\alpha_k)^{1/6}} \\ f^T(x) &= \left[1 - \left(1 + x + \frac{1}{2}x^2 + \frac{1}{6}x^3\right)e^{-x}\right] \\ f^E(x) &= \left[1 - \left(1 + x + \frac{1}{2}x^2\right)e^{-x}\right] \\ (\mathbf{r}_{jk} &= \mathbf{r}_k - \mathbf{r}_j, \quad r_{jk} = |\mathbf{r}_{jk}|) \end{aligned} \tag{2.5}$$

The standard literature parameters for the model,[32] the site polarizabilities, α_j, and the dimensionless screening parameter, a, are listed in the Supporting Information.

The complete interaction-induced series embodied in eq 2.4 is correctly infinite order in both inter- and intramolecular dipole interactions. But while it is critical to keep all orders in the intramolecular part of the series for each molecule, acetonitrile is not polarizable enough to generate significant nonlinear intermolecular contributions.[26−28] We can therefore proceed by using eq 2.4 to define the infinite-order purely intramolecular polarizabilities $\boldsymbol{\pi}^{\text{intra}}$ for both acetonitrile and C153 as the solutions of their respective self-consistent equations

$$\boldsymbol{\pi}_{ma}^{\text{intra}} = \boldsymbol{\alpha}_{ma} + \sum_{b\in m} \boldsymbol{\alpha}_{ma} \cdot \mathbf{T}_{ma,mb} \cdot \boldsymbol{\pi}_{mb}^{\text{intra}} \tag{2.6}$$

with labels such as ma referring to site a in molecule m. These intramolecular polarizabilities can then be employed in a linearized version of eq 2.4 to give us, in conjunction with eq 2.3, the final working expression for our many-body polarizabilities[35]

$$\boldsymbol{\pi}_{ma} \approx \boldsymbol{\pi}_{ma}^{\text{intra}} + \sum_{n\neq m} \sum_{b\in n} \boldsymbol{\pi}_{ma}^{\text{intra}} \cdot \mathbf{T}_{ma,nb} \cdot \boldsymbol{\pi}_{nb}^{\text{intra}} \tag{2.7}$$

(where the sums are over all sites within molecules other than the mth).

The behavior of the resulting many-body polarizabilities depends in large measure on the particular values we use for our coumarin and acetonitrile site-polarizability ingredients. How one can derive appropriate values for the ground and excited states of C153 will be the subject of section III. However, arriving at acetonitrile parameters is much more straightforward. There are already a number of published Thole models that attempt to incorporate the nonzero anisotropy of the methyl group.[40] For our purposes here, though, an isotropic methyl version will suffice. We construct our model by first using the standard literature exponential-Thole site polarizabilities[32] for H, C, and N atoms to compute the infinite-order site polarizabilities for the all-atom (6-site) model. We then identify the isotropic Me site polarizability as the sum of the average polarizabilities for each atom in the CH_3 group.

The average polarizability $\bar{\alpha}$ and polarizability anisotropy γ are, in fact, useful quantities for characterizing the polarizability of molecules as a whole

$$\begin{aligned} \bar{\alpha} &= \frac{1}{3}(\alpha_{xx} + \alpha_{yy} + \alpha_{zz}) \\ \gamma^2 &= \frac{1}{2}[(\alpha_{xx} - \alpha_{yy})^2 + (\alpha_{yy} - \alpha_{zz})^2 + (\alpha_{zz} - \alpha_{xx})^2] \end{aligned} \tag{2.8}$$

(where the xx, yy, and zz refer to the components along the principal polarizability axes). The Supporting Information reports $\bar{\alpha}$ and γ for our 3-site acetonitrile model, as well as the individual principal components of the polarizability, and compares them with experimentally measured values.[41]

C. Optical-Kerr Spectra. The full linear-response expression for the two-dimensional, solute-pump/solvent-probe response function is a three-time object bringing in the correlation between the solute−solvent potential energy at time 0 and a Poisson bracket connecting the many-body polarizabilities at times T and $T + t$.[12] However, as we noted in section I, when the time allotted for structural relaxation, T, is taken to be sufficiently large (as was actually done in the C153/acetonitrile experiment),[6,7] the signal depends only on the polarizability fluctuation time scale t. The measured response function is then simply the difference between optical-Kerr responses with the solvent equilibrated around the excited-state (e) and ground-state (g) solute:[12]

$$\Delta R(t) = R_e(t) - R_g(t) \tag{2.9}$$

$$R_n(t) = -\beta \frac{d}{dt} \langle \Pi_{xz}(0)\, \Pi_{xz}(t) \rangle_n, \quad (n = \text{e or g}) \tag{2.10}$$

(where $\beta = (k_B T)^{-1}$).

The xz subscripts here refer to those specific Cartesian components of the polarizability tensors in the laboratory frame, but the rotational invariance of the entire expression means that the response function for each solute state n can be computed more efficiently in terms of tensor invariants[42]

$$R_n(t) = -\beta \frac{d}{dt}\left[\frac{1}{10}\langle \boldsymbol{\Pi}(0) \otimes \boldsymbol{\Pi}(t) \rangle_n - \frac{1}{30}\langle \text{Tr}(\boldsymbol{\Pi}(0))\, \text{Tr}(\boldsymbol{\Pi}(t)) \rangle_n\right] \tag{2.11}$$

We shall be confining ourselves in this work to investigating the large-T limit of two-dimensional solvation spectra, so eqs 2.9 and 2.11 are the time-domain expressions we use for the remainder of the paper.

The frequency-domain equivalent of eq 2.9, the *spectral density*, is the imaginary part of its Fourier−Laplace transform

$$\text{SD}(\omega) = \int_0^\infty dt\, \sin \omega t\, \Delta R(t) \tag{2.12}$$

with analogous equations defining the individual spectral densities for the individual e and g states. But, as is traditional with OKE spectra,[15] it is also revealing to subtract off the long-time diffusive part of the signal $\Delta R^{\text{diff}}(t)$ and consider just the frequency-domain portrait of the remainder, the *reduced spectral density* (RSD),

$$\Delta R'(t) = \Delta R(t) - \Delta R^{\text{diff}}(t) \tag{2.13a}$$

dx.doi.org/10.1021/jp509021c | J. Phys. Chem. B 2015, 119, 9129−9139

$$\mathrm{RSD}(\omega) = \int_0^\infty \mathrm{d}t\ \sin \omega t\ \Delta R'(t) \tag{2.13b}$$

In practice, there is usually a clean separation of time scales between the long-time decay of the response functions and the higher frequency parts. It is therefore commonplace to derive the diffusive part empirically by fitting the long-time decay to a function of the form[43]

$$R_n^{\mathrm{diff}}(t) = (1 - \mathrm{e}^{-2\langle\nu\rangle_n t})R_n^{\mathrm{fit}}(t), \quad (n = \mathrm{e\ or\ g}) \tag{2.14a}$$

$$R_n^{\mathrm{fit}}(t) = \beta(A_1(n)\ \mathrm{e}^{-t/\tau_1(n)} + A_2(n)\ e^{-t/\tau_2(n)}) \tag{2.14b}$$

with the rise time of the diffusive portion, $\tau_{\mathrm{rise}} = (2\langle\nu\rangle)^{-1}$, set by the average spectral density (SD) frequency.

$$\langle\nu\rangle = \int \mathrm{d}\omega\ (\omega/2\pi)\ \mathrm{SD}(\omega) / \int \mathrm{d}\omega\ \mathrm{SD}(\omega) \tag{2.14c}$$

We illustrate the division between diffusive and intermolecular vibration time scales in our system and show how well the long-time dynamics is represented by fits of this sort, in Figure 2. [In this figure, the response functions are plotted as $k_B TR(t)$ (with units of Å^6/ps). In a similar fashion, all of our subsequent spectral densities are plotted as $k_B T$ times the spectral density (with units of Å^6).] Our simulation values for the rise time and diffusive-decay parameters for both ground- and excited-state C153 in acetonitrile are listed in Table 1.

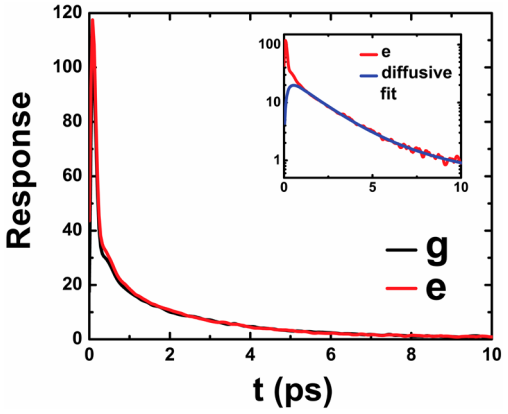

Figure 2. Calculated spectroscopic response functions for acetonitrile solutions containing ground (g) and excited (e) states of C153 (which are barely distinguishable on this scale). The inset shows a fit to the diffusive dynamics of the e-state solution.

What is left after removing the diffusive dynamics, the reduced spectral density, is most of what we care about in this work, because it is what most closely represents the change in the intermolecular vibrational spectrum of the solution when the solute is excited. Nonetheless, it is worth noting that there is also a diffusive portion of the signal resulting from the change in the solute rotational diffusion constant on electronic excitation, as evidenced by the ground-state-to-excited-state shift we see in the τ_2 values reported in Table 1. Such changes have been the subject of a number of other studies and are interesting phenomena in their own right.[44−46]

Table 1. Diffusive Portion of the Optical-Kerr-Effect Spectrum of Coumarin 153 Dissolved in Acetonitrile[a]

	coumarin ground electronic state	coumarin excited electronic state
A_1 (Å^6)	23.39	27.19
τ_1 (ps)	1.769	1.839
A_2 (Å^6)	4.164	2.075
τ_2 (ps)	6.024	10.35
τ_{rise} (ps)	0.278	0.243

[a]Parameters derived from fitting eq 2.14b to the computed long-time spectral response.

III. GROUND- AND EXCITED-STATE POLARIZABILITIES OF SOLVATION DYE MOLECULES

A. Benchmarks. Because it relies not just on the details of the electronic wave function but on its second derivative with respect to electric field, it is easy to imagine that polarizability could be a relatively difficult quantity for electronic structure methods to calculate accurately.[47] And, given that we need to find the answers for electronically excited states of fairly large dye molecules, it is natural to be concerned about the reliability of any naive quantum chemical predictions we might make for the relevant polarizabilities. Still, the demands imposed in a liquid-phase simulation context are much less onerous than they might be.

Typical solvation dyes have a fairly limited set of structural motifs and undergo relatively little geometry change on electronic excitation.[48] Moreover, the polarizability tensor supplied by a quantum chemistry calculation is not an end in itself; it is just one of the ingredients needed to parametrize a distributed multisite polarizability model. What one really wants to know is what the minimum level of electronic structure calculation that is needed to produce reasonable estimates under these circumstances, and what the magnitude and character of the likely errors are.

To provide some insight into these issues, we have carried out a number of benchmark quantum chemistry calculations on moderately sized conjugated-ring molecules that have some structural similarities to pieces of coumarin dyes, and for which both ground- and excited-state polarizability information is available. The Gaussian 09 suite of programs was used, with the polarizabilities themselves computed employing the FREQ module to calculate analytical second derivatives with respect to an electric field.[49] We display our findings in Table 2 for a single molecule, naphthalene, comparing the results for a range of different theoretical methods and basis sets with experimental data, and in Table 3 for three different molecules, *s*-tetrazine, pyrimidine, and naphthalene, limiting ourselves to a single calculational approach but assessing how different molecular species fare in comparison with literature values.[50−52]

The upshot of these tests is that, even with the smallest of our diffuse-function-containing basis sets (6-31+G(d)), ground-state polarizabilities are predicted quite well by restricted Hartree−Fock (RHF) theory and excited-state polarizabilities, though not handled quite as accurately, are still treated reasonably well using configuration interaction with single excitations (CIS).[53] Somewhat surprisingly, given that polarizability is formally the result of perturbation theory carried out to second order in an electric field (and therefore interpretable as an infinite sum over virtual states), our results seem to be amply converged with respect to basis set and show no systematic under- or overestimates of the magnitudes of either the average polarizability or the polarizability anisotropy.[54] We do note that polarizability anisotropy of the S_1 state of naphthalene is seriously overestimated at this level, but that

dx.doi.org/10.1021/jp509021c | J. Phys. Chem. B 2015, 119, 9129−9139

Table 2. Ground- and Excited-State Polarizability Tensors of Naphthalene at Different Levels of theory[a,b]

S_0	RHF/6-31+G(d)	RHF/6-31++G(d,p)	B3LYP/6-31+G(d)	RHF/aug-cc-pVDZ	expt[c]
α_{xx}	61.4	61.6	61.4	66.4	70.9
α_{yy}	114.0	112.4	120.5	129.0	119
α_{zz}	158.1	154.1	167.5	149.6	162
$\bar{\alpha}$	111.2	109.4	116.5	115.0	117
γ	83.9	80.3	92.1	75.0	78
S_1	CIS/6-31+G(d)	CIS/6-31++G(d,p)	TD-B3LYP/6-31+G(d)	CIS/aug-cc-pVDZ	expt[c]
α_{xx}	68.8	73.7	66.8	77.1	76.9
α_{yy}	127.8	125.4	138.2	130.1	120
α_{zz}	232.9	231.3	329.1	235.2	187
$\bar{\alpha}$	143.2	143.5	178.0	147.5	128
γ	144.0	139.2	235.0	139.4	96

[a]Principal components of the polarizability tensor (α_{xx}, α_{yy}, and α_{zz}), average polarizability ($\bar{\alpha}$), and polarizability anisotropy (γ) of napthalene reported in atomic units (1 au = 0.14818 Å^3) for the electronic ground (S_0) and first-excited (S_1) states. [b]Results from electronic structure calculations using the indicated methods are given in the first four columns. The molecular geometries used in these calculations are optimized at the B3LYP/6-31++G(d,p) for the first three columns and at the RHF/aug-cc-pVDZ level for the fourth column. [c]Experimental values are taken from ref 50.

Table 3. *s*-Tetrazine, Pyrimidine, and Naphthalene. Comparison of Ground- and Excited-State Polarizability Tensors with Literature Results[a,b,c]

S_0	*s*-tetrazine	pyrimidine	napthalene
α_{xx}	28.12 (32.0)	32.57 (37.0)	61.41 (70.5)
α_{yy}	51.45 (54.4)	61.78 (67.9)	114.92 (118.9)
α_{zz}	55.72 (59.0)	63.61 (70.6)	158.13 (161.2)
$\bar{\alpha}$	45.10 (48.5)	52.65 (56.5)	111.48 (116.9)
γ	25.73 (25.0)	30.17 (30.2)	83.92 (78.6)
S_1	*s*-tetrazine	pyrimidine	napthalene
α_{xx}	27.00 (31.3)	38.55 (41.3)	68.78 (76.6)
α_{yy}	61.28 (63.9)	65.89 (71.8)	127.77 (119.6)
α_{zz}	69.28 (74.0)	94.90 (107.2)	232.86 (186.1)
$\bar{\alpha}$	52.52 (56.4)	66.45 (73.4)	143.14 (127.4)
γ	38.91 (38.7)	48.80 (57.1)	143.95 (95.6)

[a]Principal components of the polarizability tensor (α_{xx}, α_{yy}, and α_{zz}), average polarizability ($\bar{\alpha}$), and polarizability anisotropy (γ) reported in atomic units (1 au = 0.14818 Å^3) for the electronic ground (S_0) and first-excited (S_1) states of the indicated molecules. [b]The first value for each entry reports this work's electronic structure result with geometry optimized on the ground state at the B3LYP/6-31++G(d,p) level and the polarizability calculated at the RHF/6-31+G(d) and CIS/6-31+G(d) levels for the S_0 and S_1 states, respectively. [c]Values in parentheses are literature results: for *s*-tetrazine, an equation-of-motion CCSD calculation (ref 51); for pyrimidine, a DFT calculation (ref 52); and for naphthalene, an experimental measurement (ref 50).

Table 4. Ground- and Excited-State Polarizability Tensors of Coumarin 153[a]

S_0	Thole (lit. params)[b]	quantum chem[c]	Thole (this work)[d]
α_{xx}	124.3	115.0	116.0
α_{yy}	199.4	210.4	210.4
α_{zz}	221.7	255.4	255.0
$\bar{\alpha}$	181.8	193.6	193.8
γ	88.4	124.2	122.9
% error[e]	19%		0.6%
S_1	Thole (lit. params)[b]	quantum chem[c]	Thole (this work)[d]
α_{xx}	124.3	126.6	151.2
α_{yy}	199.4	220.4	237.7
α_{zz}	221.7	349.8	328.4
$\bar{\alpha}$	181.8	232.3	239.1
γ	88.4	194.1	153.5
% error[e]	56%		16%

[a]Principal components of the polarizability tensor (α_{xx}, α_{yy}, and α_{zz}), average polarizability ($\bar{\alpha}$), and polarizability anisotropy (γ) reported in atomic units (1 au = 0.14818 Å^3) for the electronic ground (S_0) and first-excited (S_1) states of C153. [b]Exponential Thole model using literature parameters. [c]Electronic structure results calculated as described in the text. [d]Exponential Thole model using parameters fit to the quantum chemistry results in this table. [e]The fractional error, defined to be the fractional root-mean-square deviation of the average polarizability from the quantum chemistry results (and reported here as a percentage: $100\Phi/\bar{\alpha}$).

problem does not seem to recur in the excited states of the other molecules we examined.

Guided by these findings, we will be making use of the 6-31+G(d) basis at the RHF and CIS levels to calculate the necessary polarizability tensors for our coumarin solute.

B. Modeling the Ground- and Excited-State Polarizability of Coumarin 153. With this level of theory (optimizing the geometry for both e and g states at the ground-state minimum determined at the B3LYP/6-31++G(d,p) level), we predict that the ground- and excited-state polarizability tensors of C153 should differ significantly (Table 4). Electronic excitation increases the average polarizability by 20% and the polarizability anisotropy by more than 50%.

It is worth pointing out how different the quantum-chemistry-predicted polarizabilities are from those assumed in traditional liquid-state simulation models (Table 4). Using the exponential Thole model with standard literature parameters (Supporting Information Table S5) for the constituent atoms, for example,[32] leads to a reasonably accurate portrait of the average ground-state polarizability, but it generates a ground-state polarizability anisotropy that is almost 30% too small. More to the point, since this model fails to allow for changes on electronic excitation, it fares even worse in its excited-state prediction: the excited-state polarizability anisotropy is less than half of what it needs to be.

The root cause of the discrepancies is apparently not the use of the exponential Thole model with individual site polarizabilities on each atom; rather, it is the need to make appropriate (and different) choices for the site-polarizability

dx.doi.org/10.1021/jp509021c | J. Phys. Chem. B 2015, 119, 9129−9139

Table 5. Newly Developed Exponential Thole Model Site Polarizabilities for the Ground and First-Excited Electronic States of Coumarin 153[a]

S_0			S_1		
site	specific atoms	α	site	specific atoms	α
C−	2, 3, 5, 8, 11	19.7839	C−	2, 5, 8, 11	22.9039
			C0	1, 3, 6, 15, 18, 24, 27	19.0539
C+	all other C's	7.7739	C+	4, 10, 14, 23, 33	0.6739
N	13	19.1404	N	13	14.2704
O	9, 12	6.8380	O	9, 12	21.6480
H	all H's	0.0001	H	all H's	0.0001
F	34−36	3.0228	F	34−36	3.0228

[a]Electronic ground-state (S_0) and first-excited-state (S_1) site polarizabilities α for each of the atoms in C153, reported in atomic units (1 au = 0.14818 Å^3).

values of the ground and excited states. From that perspective, the optimum site values for C153 are going to be those that minimize the root-mean-square deviation of the quantum-chemistry answer, $\boldsymbol{\alpha}$(QM), from the net intramolecular Thole polarizability tensor $\boldsymbol{\pi}^{\text{intra}}$(Thole)

$$\boldsymbol{\pi}^{\text{intra}}(\text{Thole}) = \sum_a \boldsymbol{\pi}_a^{\text{intra}} \tag{3.1}$$

(with the sum over all of the coumarin sites and each site contribution $\boldsymbol{\pi}_a^{\text{intra}}$ given by eq 2.6). The root-mean-square deviation Φ can then be defined in terms of the principal components μ of $\boldsymbol{\pi}^{\text{intra}}$.

$$\Phi = \sqrt{\sum_{\mu=x,y,z} (\alpha_{\mu\mu}(\text{QM}) - \pi_{\mu\mu}^{\text{intra}}(\text{Thole}))^2} \tag{3.2}$$

It makes sense on physical grounds to look for solutions that group identical atoms together. We therefore restricted our search for optimum site polarizabilities to parameter sets in which all 14 H atoms have the same value, all 3 F atoms have the same value, and both O atoms have the same value. However, the wide variation in charge density among the different carbon atoms suggested that there might be a comparable variability in the polarizabilities. Indeed, we noticed that we could considerably improve our fits by allowing C atoms with different quantum-chemistry-derived site charges[30,55] (Supporting Information Table S4) to take on different site polarizabilities. We found, for example, that for C atoms with significant negative site charges (which we shall call C− sites), the literature Thole values were too small, and for C atoms with significant positive site charges (denoted C+), the literature values were too large. The optimum site polarizabilities we ended up with are listed in Table 5 for both the ground and excited state of C153. The overall molecular polarizability tensor calculated using these values is compared with that implied by the standard literature site values, and with the answer derived from quantum chemistry, in Table 4.

The polarizability models we derived in this section are clearly much more faithful representations of *ab initio* quantum chemical expectations for the ground and excited states of our solvation dye than are traditional models. The ground-state polarizability tensor of C153 is reproduced virtually exactly, and the changes on going to the excited state are handled, if not perfectly, at least respectably. (The most notable error for the excited state is the 20% underestimate of the polarizability anisotropy; the average polarizability is reproduced within a few percent.) The *ab initio* results behind these models are also likely to be more accurate than the semiempirical calculations currently in the literature. While the published semiempirical predictions for the average polarizabilities of the S_0 and S_1 states of C153 (23.4 and 35.7 Å^3, respectively)[24] are actually not too far from our *ab initio* results (28.7 and 34.4 Å^3), our benchmark studies suggest the latter should be quantitative. We are therefore ready to proceed with calculating the spectroscopy with our models.

By way of prefacing that calculation, though, we should note the magnitude and geometry of the polarizability changes that we can now say are behind that spectroscopy. Figure 3 portrays the individual site-polarizability and overall-polarizability-tensor changes predicted by our new Thole model.

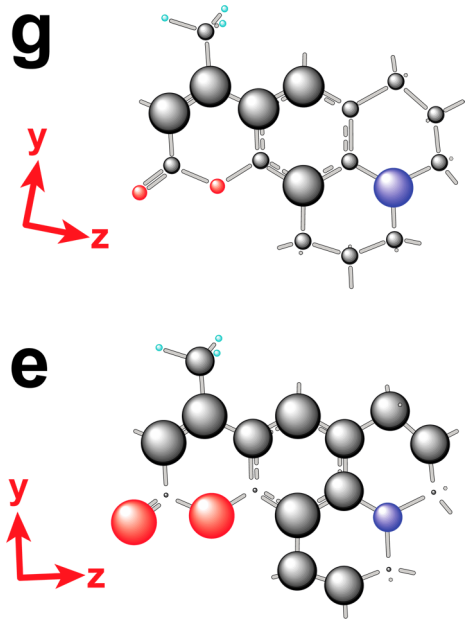

Figure 3. Our model's principal in-plane polarizability axes (indicated by arrows) and site-polarizability magnitudes (indicated by the relative sizes of the spheres) for ground (g) and excited state (e) C153. Atom locations are identical to those shown in Figure 1.

Substantial changes evidently occur in the oxygen atoms (red), the nitrogen atom (blue), and carbons with a positive site charge. Despite these shifts, the change in the direction of the principal polarizability axes is fairly subtle, mostly a small (12°) rotation of the two in-plane (**y** and **z**) axes about an axis perpendicular to the aromatic plane (**x**). We turn now to the spectroscopic implications of these changes.

dx.doi.org/10.1021/jp509021c | J. Phys. Chem. B 2015, 119, 9129−9139

IV. SOLUTE-PUMP/SOLVENT-PROBE SPECTROSCOPY

A. Simulation Details. The spectra we report in this work were computed via an *NVE* molecular dynamics simulation of the terms in eqs 2.9−2.11, an approach that correctly represents (non-quantum-mechanical aspects of) the spectra in the long-structural-relaxation-time limit. Rigid-body rotations were handled by quaternions, and the equations of motion were integrated via leapfrog Verlet method with a time step of 2 fs. Simulations were run with cubic periodic boundary conditions with Ewald summation used to treat the long-ranged electrostatic interactions. Lennard-Jones potentials were cut off at 13.0 Å.[56a,b]

In order to ensure that our study was carried out at a thermodynamic state appropriate to the 1 atm and 300 K conditions of the Scherer group's recent experiments,[6,7] we adopted the following protocol: The first 100 ps of our simulations were performed for our 244 acetonitrile, 1 C153 system in the *NpT* ensemble using the Berendsen thermostat and barostat[57] to set the pressure p to 1 atm and the temperature T to 300 K. Using the average simulation volume determined by this run (26.77 Å^3), we then carried out a 100 ps simulation in the *NVT* ensemble using just the Berendsen thermostat[57] (rescaling velocities in the first 10 ps of both 100 ps segments in order to achieve the desired 300 K temperature). Final equilibration and data collection were carried out in the *NVE* ensemble. For both the ground- and excited-state simulations, equilibration runs of 1 ns preceded the actual data collection. The requisite spectroscopic correlation functions were derived from 10 ns trajectories, recording data every 20 time steps, so that results are averaged over 2.5 × 10^5 configurations.

B. Results. Although it is difficult to see the change in OKE response functions between acetonitrile solutions equilibrated with ground-state C153 (g) and excited-state C153 (e) (Figure 2), the differences become quite visible in the spectral density (Figure 4) and reduced spectral density (Figure 5). Moreover, the difference spectrum (e−g) spans a frequency range extending noticeably beyond the 250 cm^{-1} or so expected for neat liquid acetonitrile.[26,27,58,59]

For frequencies larger than 50 cm^{-1}, the predicted experimental spectrum (Figure 4, bottom panel) scarcely changes when the diffusive dynamics is subtracted out (Figure 5, bottom panel), emphasizing that the vast majority of the signal indeed arises from solute-excitation-induced changes in the solution's intermolecular vibrational dynamics. But exactly what parts of that dynamics are most visible? We can obtain answers to this question fairly directly by performing a component-by-component analysis[26,40,60] of the spectral response with ground- (g) and excited-state (e) solutes (Figure 6).

To carry out this analysis, each site contribution to the many-body polarizabilities $\boldsymbol{\pi}_m$ appearing in eq 2.7 is considered to be a sum of single-molecule ($\boldsymbol{\pi}_m^{\mathrm{intra}}$), and interaction-induced parts ($\boldsymbol{\pi}_m^{\mathrm{intra}}\cdot\mathbf{T}_{mn}\cdot\boldsymbol{\pi}_n^{\mathrm{intra}}$). The single-molecule terms are then partitioned into solute (**u**) and solvent (**v**) components, and the interaction-induced terms divided into solute−solute, solute−solvent, and solvent−solvent components (**uu**, **uv**, and **vv**, respectively). When these polarizabilities are substituted into the response functions, eq 2.11, the resulting spectra are resolved into a number of different kinds of contributions: Components derived from autocorrelations of these components are simply denoted by **u**, **v**, **uu**, **uv**, and **vv**, respectively.

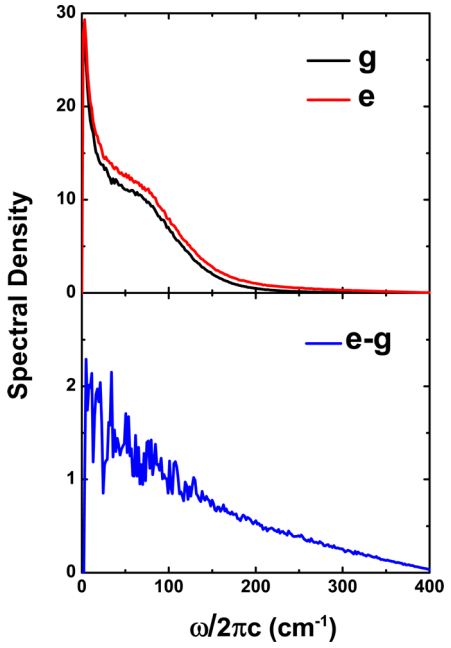

Figure 4. Spectral density for C153/acetonitrile solutions. The top panel shows results for the ground (g) and excited-state (e) solutions; the bottom panel shows our predicted solute-pump/solvent-probe spectrum.

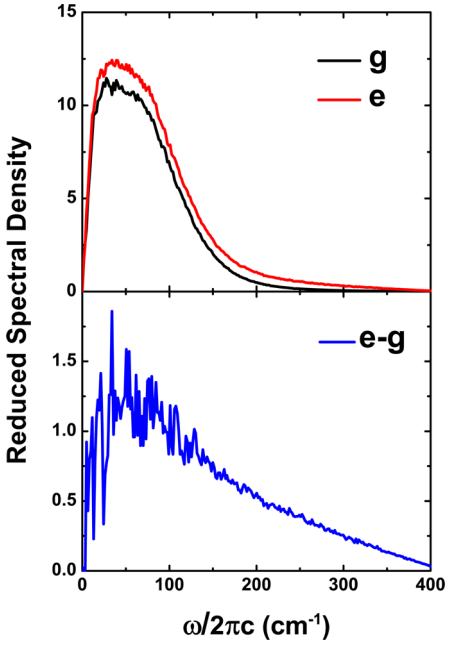

Figure 5. Reduced spectral density for C153/acetonitrile solutions. The top panel shows results for the ground (g) and excited-state (e) solutions; the bottom panel shows the difference spectrum.

Cross terms between components are indicated by placing a comma between the two contributing pieces. For example (**v**, **vv**) denotes the cross-correlation between dynamics modulating the single-solvent polarizability and dynamics affecting the solvent−solvent interaction-induced polarizability. Since our single molecule polarizability tensors are constant (in the molecular frame), any single-molecule dynamics has to come entirely from molecular reorientation. The interaction-induced terms, on the other hand, will become visible when either the

dx.doi.org/10.1021/jp509021c | J. Phys. Chem. B 2015, 119, 9129−9139

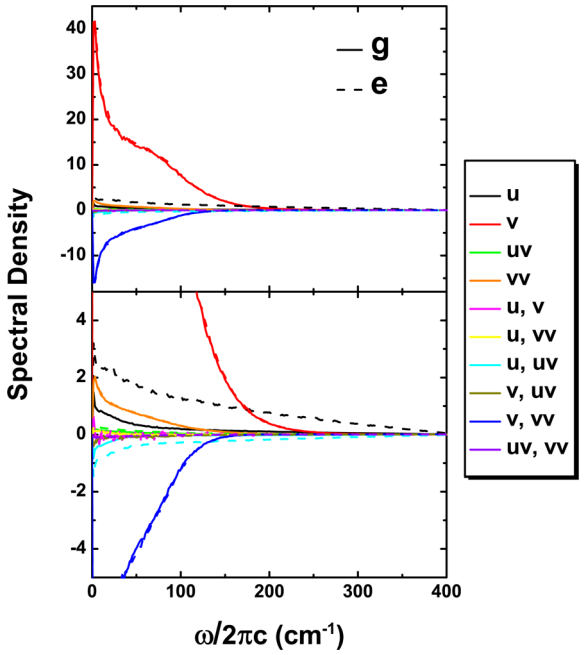

Figure 6. Leading components of the many-body polarizability contributing to the spectral density of C153/acetonitrile solutions (magnified view in the bottom panel).

intermolecular distance changes with time (changing the **T** tensors) or one or more of the contributing species reorients.

Figure 6 makes it clear that the individual ground- and excited-state spectra come almost exclusively from the solvent dynamics, in particular from the solvent libration (**v**) and from the coupling between solvent libration and the dynamics governing the solvent−solvent interaction-induced polarizability (**v**, **vv**). However, exciting the solute fails to produce any change, at least on this scale, in either of those contributions. The solute-pump/solvent-probe signal, by contrast (Figure 7)

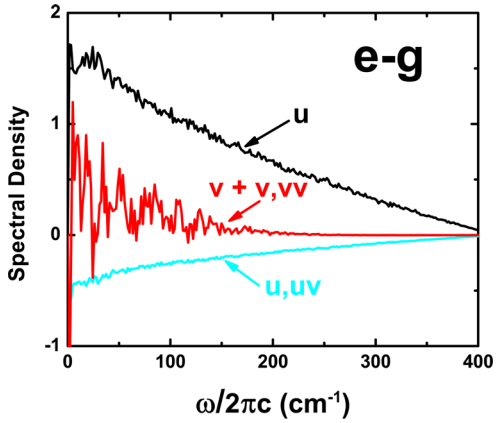

Figure 7. Leading components of the many-body polarizability contributing to the solute-pump/solvent-probe spectrum of C153/acetonitrile solutions.

explicitly looks at the effects of the excitation. That spectrum seems to be focused on the region near the solute, with the principal contributions now the solute's own libration (**u**) and the dynamics affecting the correlation between solute's polarizability and the solute−solvent interaction-induced polarizabilities (**u**, **uv**).

The origins of this focus on the solute are worth pursuing in a little more depth. We know from prior work that excitation of the solute does produce local changes in the dynamics of the solvent, much of it in the first solvation shell.[12,13] But it is the simultaneous change in the polarizability of the solute that allows us to see that shift in the dynamics. Suppose, for example (Figure 8), we were to recalculate the g and e solution spectral

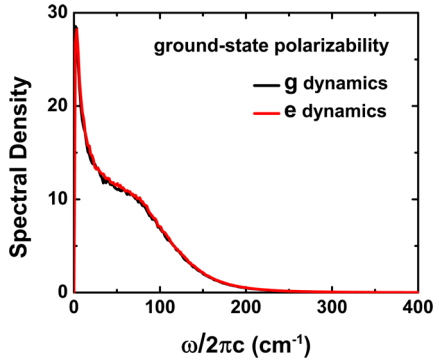

Figure 8. Spectral density for C153/acetonitrile solutions with identical g and e-state coumarin polarizabilities.

densities with the correct dynamics in each case, but with the solute polarizability kept in its g state. That is, suppose we were to continue to include the correctly distinct partial charges of the g-state solute and e-state solute in our intermolecular potentials, eq 2.1, when solving the equations of motion for solutions containing solutes in these respective states, but at the same time neglected to include the dependence of the spectroscopic observable, the solution's polarizability, on the solute's electronic state.

The difference between the two spectral densities that was visible in the top panel of Figure 4 seems to be virtually absent when the polarizability difference is turned off.

To see this point another way, we could also imagine keeping the g- and e-state polarizabilities the same while changing the magnitude of that polarizability. The sizes of the **u**, (**u**, **uv**), and (**uv**, **uv**) components of the response function increase with the square of the solute's polarizability whereas all of the other components shown in Figure 6 increase no faster than linearly. Since we know from Figure 7 that it is possible to see e − g dynamical differences in the **u** and (**u**, **uv**) components, one might expect that simply increasing the magnitude of the solute's polarizability might be enough to render the electronic-state-change-induced dynamics easily visible, even if the polarizability were not state-dependent. Figure 9, though, suggests otherwise.

The calculations here took (electronic-state-independent) literature values for the C153 exponential-Thole site polarizabilities[32] (rather than the ones developed in section III) and then scaled the resulting single-molecule infinite-order polarizabilities by factors of 0, 1, and 10. Neither the zero-solute polarizability case nor the literature-valued case displays any discernible difference between the spectral responses for g and e states. In fact, all four curves (zero and standard-literature polarizabilities; ground and excited states) are virtually indistinguishable on this scale. The absolute size of the spectral response does become noticeably larger when the polarizability magnitude is increased by a factor of 10 (although only by a factor of 2), and we finally do start to see small dynamical differences between the different electronic states, but to a

dx.doi.org/10.1021/jp509021c | J. Phys. Chem. B 2015, 119, 9129−9139

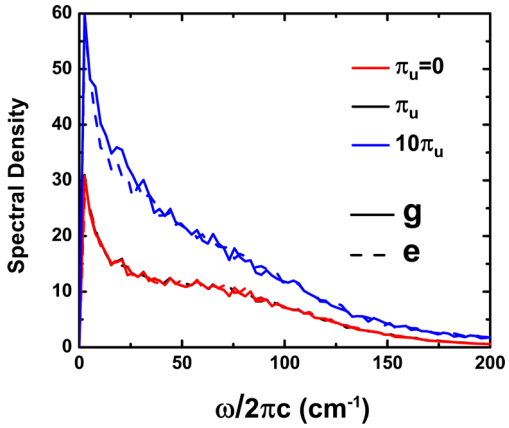

Figure 9. Effect of changing the magnitude of the coumarin polarizability (π_u) on the spectral density for C153/acetonitrile solutions with identical g- and e-state coumarin polarizabilities.

lesser degree than that seen for the much smaller and more realistic polarizabilities used to generate the top panel of Figure 4. Evidently state-to-state polarizability changes are among the more valuable features of the dyes used in solvation experiments; at least in a polarizability-sensitive spectroscopy, they act to amplify the spectroscopic signatures of the differing dynamics occurring with different solute states.

We bring this section to a close by comparing our predictions for the long-T limit of the solute-pump/solvent-probe spectrum of our system to actual measurements for C153 in acetonitrile. Shown in Figure 10 is our spectral density taken from the lower

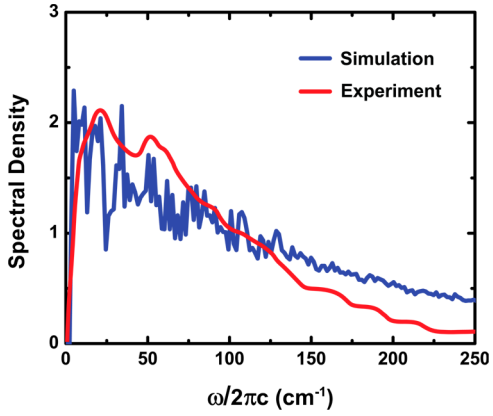

Figure 10. Comparison between simulated and experimental solute-pump/solvent-probe spectra for C153 dissolved in acetonitrile.

panel of Figure 4 and the T = 4 ps RP-PORS anisotropic experimental results presented by Park et al.[6] (scaled to match the simulated peak height). RP-PORS signals can be either positive or negative, so the overall agreement in sign, shape, and spectral region between the experimental and theoretical curves is worth noting. We probably cannot expect a close match at the higher frequencies ($\omega/2\pi c$ > 200 cm^{-1}) given that our model for C153 is completely rigid, but that aside, the correspondence with experimental data certainly lends support to our conceptual and computational picture of this kind of spectroscopy.

V. CONCLUDING REMARKS

This work reports the first molecularly detailed calculation of the solute-pump/solvent-probe spectrum corresponding to an experimental measurement. Performing this calculation required that we capture not only how each atomic site in both the ground and excited electronic states of the solute interacts with the solvent but also how the polarizability at each solute site is affected by the change in electronic state. Determining the latter, though, proved to be well within the reach of routine electronic structural methods. As evidenced by a number of benchmark studies on smaller aromatic ring species, both ground- and first-excited-state polarizability tensors seem to be available to an adequate level of accuracy for the kinds of dyes typically used in solvation studies—and turning those tensors into individual site polarizabilities of the type useful in liquid simulations ended up not being that arduous.

We evaluated our spectra only in the long-structural-relaxation-time limit. However, that turned out to be sufficient to make clear what it was that these spectra were seeing. Since solute-pump/solvent-probe spectra measure the effects of solute excitation on the solvent, it is not surprising that these spectra focus on the solvent dynamics in the vicinity in the solute. What this work points out, though, is how the apparent complication that the solute's electronic excitation affects both the system's dynamics (via the intermolecular interaction change) and the spectroscopic readout of that dynamics (via the solute polarizability change) is actually an advantage. The polarizability increase effectively lights up the excited-state solute libration and the coupled excited-state solute/solvent dynamics. The excitation-induced dynamics therefore becomes much easier to see against the backdrop of unperturbed ground-state dynamics that it otherwise would have been.

While we believe that the study in this work was revealing, it is worth emphasizing that the coumarin/acetonitrile system we studied here (and the limit we studied it in) does not come close to illustrating the full potential of this spectroscopy. The real promise of these spectra is that they can look simultaneously at ultrafast dynamics and slower solvent structural changes.[13] Acetronitrile simply does not exhibit much structural change when it solvates C153. But, when structural changes do occur, as they do with preferential solvation,[20,22,23] our previous work suggests that traditional time-dependent-fluorescence measurements (which are limited to following the dynamics of the solute−solvent interaction) will not be able to portray the structural evolution nearly as well as the full two-dimensional version of solute-pump/solvent-probe spectroscopy. The fact that electronic excitation changes more than the solute−solvent interaction opens a new window onto the solution dynamics.

■ ASSOCIATED CONTENT

Supporting Information

Tables listing details on our acetonitrile and coumarin 153 potential models, our acetonitrile polarizability model, and a selected list of standard literature polarizability parameters. This material is available free of charge via the Internet at http://pubs.acs.org.

■ AUTHOR INFORMATION

Corresponding Authors

*(B.M.L.) Phone: +1 970 491 5196. E-mail: Branka.Ladanyi@colostate.edu.

dx.doi.org/10.1021/jp509021c | J. Phys. Chem. B 2015, 119, 9129−9139

*(R.M.S.) Phone: +1 401 863 3418. E-mail: Richard_Stratt@brown.edu.

Notes

The authors declare no competing financial interest.

■ ACKNOWLEDGMENTS

This work was partially supported by National Science Foundation Grant Nos. CHE-1213682 (B.M.L.) and CHE-1265798 (R.M.S.). We thank Margaret Hershberger for continuing discussion about this spectroscopy, Norbert Scherer and Sungnam Park for freely sharing their insights and experimental results over the past decade, and Xinxin Cheng for her assistance with the Gaussian calculations.

■ REFERENCES

(1) Park, S.; Flanders, B. N.; Shang, X.; Westervelt, R. A.; Kim, J.; Scherer, N. F. Solvent Intermolecular Polarizability Response in Solvation. *J. Chem. Phys.* **2003**, *118*, 3917−3920.
(2) Park, S.; Kim, J.; Scherer, N. F. In *Ultrafast Phenomena XIV*; Kobayashi, T., Okada, T., Kobayashi, T., Nelson, K. A., De Silvestri, S., Eds.; Springer: New York, 2005; pp 557−559.
(3) Moran, A. M.; Park, S.; Scherer, N. F. Coherent Electronic and Nuclear Dynamics for Charge Transfer in 1-Ethyl-4-(carbomethoxy)-pyridinium Iodide. *J. Phys. Chem. B* **2006**, *110*, 19771−19783.
(4) Moran, A. M.; Nome, R. A.; Scherer, N. F. Field-Resolved Measurement of Reaction-Induced Spectral Densities by Polarizability Response Spectroscopy. *J. Chem. Phys.* **2007**, *127*, No. 184505.
(5) Moran, A. M.; Park, S.; Scherer, N. F. Polarizability Response Spectroscopy: Formalism and Simulation of Ultrafast Dynamics in Solvation. *Chem. Phys.* **2007**, *341*, 344−356.
(6) Park, S.; Kim, J.; Moran, A. M.; Scherer, N. F. Solvent Structural Relaxation Dynamics in Dipolar Solvation Studied by Resonant Pump Polarizability Response Spectroscopy. *Phys. Chem. Chem. Phys.* **2011**, *13*, 214−223.
(7) Park, S.; Kim, J.; Scherer, N. F. Two-Dimensional Measurements of the Solvent Structural Relaxation Dynamics in Dipolar Solvation. *Phys. Chem. Chem. Phys.* **2012**, *14*, 8116−8122.
(8) Underwood, D. F.; Blank, D. A. Ultrafast Solvation Dynamics: A View from the Solvent's Perspective Using a Novel Resonant-Pump, Nonresonant-Probe Technique. *J. Phys. Chem. A* **2003**, *107*, 956−961; **2003**, *107*, 9736−9736.
(9) Schmidtke, S. J.; Underwood, D. F.; Blank, D. A. Following the Solvent Directly during Ultrafast Excited State Proton Transfer. *J. Am. Chem. Soc.* **2004**, *126*, 8620−8621.
(10) Underwood, D. F.; Blank, D. A. Measuring the Change in the Intermolecular Raman Spectrum during Dipolar Solvation. *J. Phys. Chem. A* **2005**, *109*, 3295−3306.
(11) Schmidtke, S. J.; Underwood, D. F.; Blank, D. A. Probing Excited-State Dynamics and Intramolecular Proton Transfer in 1-Acylaminoanthraquinones via the Intermolecular Solvent Response. *J. Phys. Chem. A* **2005**, *109*, 7033−7045.
(12) Sun, X.; Stratt, R. M. The Molecular Underpinnings of a Solute-Pump/Solvent-Probe Spectroscopy: The Theory of Polarizability Response Spectra and an Application to Preferential Solvation. *Phys. Chem. Chem. Phys.* **2012**, *14*, 6320−6331.
(13) Sun, X.; Stratt, R. M. How a Solute-Pump/Solvent-Probe Spectroscopy Can Reveal Structural Dynamics: Polarizability Response Spectra as a Two-Dimensional Solvation Spectroscopy. *J. Chem. Phys.* **2013**, *139*, No. 044506.
(14) Hunt, N. T.; Jaye, A. A.; Meech, S. R. Ultrafast Dynamics in Complex Fluids Observed through the Ultrafast Optically-Heterodyne-Detected Optical-Kerr-Effect (OHD-OKE). *Phys. Chem. Chem. Phys.* **2007**, *9*, 2167−2180.
(15) Zhong, Q.; Fourkas, J. T. Optical Kerr Effect Spectroscopy of Simple Liquids. *J. Phys. Chem. B* **2008**, *112*, 15529−15539.
(16) Stratt, R. M.; Maroncelli, M. Nonreactive Dynamics in Solution: The Emerging Molecular View of Solvation Dynamics and Vibrational Relaxation. *J. Phys. Chem.* **1996**, *100*, 12981−12996.
(17) Horng, M. L.; Gardecki, J. A.; Papazyan, A.; Maroncelli, M. Subpicosecond Measurements of Polar Solvation Dynamics: Coumarin 153 Revisited. *J. Phys. Chem.* **1995**, *99*, 17311−17337.
(18) Eom, I.; Joo, T. Polar Solvation Dynamics of Coumarin 153 by Ultrafast Time-Resolved Fluorescence. *J. Chem. Phys.* **2009**, *131*, No. 244507.
(19) Sajadi, M.; Ernsting, N. P. Excess Dynamic Stokes Shift of Molecular Probes in Solution. *J. Phys. Chem. B* **2013**, *117*, 7675−7684.
(20) Nguyen, C. N.; Stratt, R. M. Preferential Solvation Dynamics in Liquids: How Geodesic Pathways through the Potential Energy Landscape Reveal Mechanistic Details about Solute Relaxation in Liquids. *J. Chem. Phys.* **2010**, *133*, No. 124503.
(21) Luther, B. M.; Kimmel, J. R.; Levinger, N. E. Dynamics of Polar Solvation in Acetonitrile-Benzene Binary Mixtures: Role of Dipolar and Quadrupolar Contributions to Solvation. *J. Chem. Phys.* **2002**, *116*, 3370−3377.
(22) Ladanyi, B. M.; Perng, B.-C. Solvation Dynamics in Dipolar−Quadrupolar Mixtures: A Computer Simulation Study of Dipole Creation in Mixtures of Acetonitrile and Benzene. *J. Phys. Chem. A* **2002**, *106*, 6922−6934.
(23) Martins, L. R.; Tamashiro, A.; Laria, D.; Skaf, M. S. Solvation Dynamics of Coumarin 153 in Dimethylsulfoxide-Water Mixtures: Molecular Dynamics Simulations. *J. Chem. Phys.* **2003**, *118*, 5955−5963.
(24) Cichos, F.; Brown, R.; Bopp, P. A. Coupled Molecular Dynamics/Semiempirical Simulation of Organic Solutes in Polar Liquids. II. Coumarin 153 in Methanol and Acetonitrile. *J. Chem. Phys.* **2001**, *114*, 6834−6842.
(25) Geiger, L. C.; Ladanyi, B. M. Higher-Order Interaction-Induced Effects on the Allowed Raman-Spectra of Liquid CS_2. *J. Chem. Phys.* **1988**, *89*, 6588−6599.
(26) Ladanyi, B. M.; Klein, S. Contributions of Rotation and Translation to Polarizability Anisotropy and Solvation Dynamics in Acetonitrile. *J. Chem. Phys.* **1996**, *105*, 1552−1561.
(27) Elola, M. D.; Ladanyi, B. M. Polarizability Response in Polar Solvents: Molecular-Dynamics Simulations of Acetonitrile and Chloroform. *J. Chem. Phys.* **2005**, *122*, No. 224506.
(28) Milischuk, A. A.; Ladanyi, B. M. Polarizability Anisotropy Relaxation in Nanoconfinement: Molecular Simulation Study of Acetonitrile in Silica Pores. *J. Phys. Chem. B* **2013**, *117*, 15729−15740.
(29) Kumar, P. V.; Maroncelli, M. Polar Solvation Dynamics of Polyatomic Solutes—Simulation Studies in Acetonitrile and Methanol. *J. Chem. Phys.* **1995**, *103*, 3038−3060.
(30) Ingrosso, F.; Ladanyi, B. M.; Mennucci, B.; Elola, M. D.; Tomasi, J. Solvation Dynamics in Acetonitrile: A Study incorporating Solute Electronic Response and Nuclear Relaxation. *J. Phys. Chem. B* **2005**, *109*, 3553−3564.
(31) Thole, B. T. Molecular Polarizabilities Calculated with a Modified Dipole Interaction. *Chem. Phys.* **1981**, *59*, 341−350.
(32) van Duijnen, P. T.; Swart, M. Molecular and Atomic Polarizabilities: Thole's Model Revisited. *J. Phys. Chem. A* **1998**, *102*, 2399−2407.
(33) Swart, M.; van Duijnen, P. T.; Snijders, J. G. Mean Polarizabilities of Organic Molecules. A Comparison of Restricted Hartree Fock, Density Functional Theory and Direct Reaction Field Results. *J. Mol. Struct. (THEOCHEM)* **1999**, *458*, 11−17.
(34) Jansen, T. L. C.; Swart, M.; Jensen, L.; van Duijnen, P. T.; Snijders, J. G.; Duppen, K. Collision Effects in the Nonlinear Raman Response of Liquid Carbon Disulfide. *J. Chem. Phys.* **2002**, *116*, 3277−3285.
(35) Lupi, L.; Comez, L.; Paolantoni, M.; Fioretto, D.; Ladanyi, B. M. Dynamics of Biological Water: Insights from Molecular Modeling of Light Scattering in Aqueous Trehalose Solutions. *J. Phys. Chem. B* **2012**, *116*, 7499−7508.
(36) Jorgensen, W. L.; Maxwell, D. S.; Tirado-Rives, J. Development and Testing of the OPLS All-Atom Force Field on Conformational

Energetics and Properties of Organic Liquids. *J. Am. Chem. Soc.* **1996**, *118*, 11225−11236.
(37) Gee, P. J.; van Gunsteren, W. F. Acetonitrile Revisited: A Molecular Dynamics Study of the Liquid Phase. *Mol. Phys.* **2006**, *104*, 477−483.
(38) Jorgensen, W. L.; Schyman, P. Treatment of Halogen Bonding in the OPLS-AA Force Field: Application to Potent Anti-HIV Agents. *J. Chem. Theory Comput.* **2012**, *8*, 3895−3901.
(39) Mukamel, S. *Principles of Nonlinear Optical Spectroscopy*; Oxford: New York, 1995; Chapter 15.
(40) Paolantoni, M.; Ladanyi, B. M. Polarizability Anisotropy Relaxation in Liquid Ethanol: A Molecular Dynamics Study. *J. Chem. Phys.* **2002**, *117*, 3856−3873.
(41) Alms, G. R.; Burnham, A. K.; Flygare, W. H. Measurement of Dispersion in Polarizability Anisotropies. *J. Chem. Phys.* **1975**, *63*, 3321−3326.
(42) Murry, R. L.; Fourkas, J. T. Polarization Selectivity of Nonresonant Spectroscopies in Isotropic Media. *J. Chem. Phys.* **1997**, *107*, 9726−9740.
(43) Rajian, J. R.; Hyun, B.-R.; Quitevis, E. L. Intermolecular Spectrum of Liquid Biphenyl Studied by Optical Kerr Effect Spectroscopy. *J. Phys. Chem. A* **2004**, *108*, 10107−10115.
(44) Reiser, D.; Laubereau, A. Effect of Electronic Excitation on Ultrafast Rotational Motion of Dye Molecules. *Chem. Phys. Lett.* **1982**, *92*, 297−301.
(45) Gaab, K. M.; Bardeen, C. J. Nonstationary Rotational Diffusion in Room Temperature Liquids Measured by Femtosecond Three-Pulse Transient Anisotropy. *Phys. Rev. Lett.* **2004**, *93*, No. 056001.
(46) Zhou, P.; Song, P.; Liu, J.; Shi, Y.; Han, K.; He, G. Rotational Reorientation Dynamics of Oxazine 750 in Polar Solvents. *J. Phys. Chem. A* **2008**, *112*, 3646−3655. Zhou, P.; Liu, J.; Song, P.; Han, K.; He, G. Rotational Reorientation Dynamics of Rhodamine 700 in Different Excited States. *J. Lumin.* **2009**, *129*, 283−289.
(47) Dykstra, C. E. Dipole (Electric-Field) and Quadrupole (Field Gradient) Polarizabilities of Hydrogen, Nitrogen, and Acetylene from the Application of Derivative Hartree-Fock Theory. *J. Chem. Phys.* **1985**, *82*, 4120−4125. Liu, S.; Dykstra, C. E. Multipole Polarizabilities and Hyperpolarizabilities of AH_n and A_2H_n Molecules from Derivative Hartree-Fock Theory. *J. Phys. Chem.* **1987**, *91*, 1749−1754.
(48) Cave, R. J.; Castner, E. W., Jr. Time-Dependent Density Functional Theory Investigation of the Ground and Excited States of Coumarins 102, 152, 153, and 343. *J. Phys. Chem. A* **2002**, *106*, 12117−12123.
(49) Frisch, M. J.; Trucks, G. W.; Schlegel, H. B.; Scuseria, G. E.; Robb, M. A.; Cheeseman, J. R.; Scalmani, G.; Barone, V.; Mennucci, B.; Petersson, G. A.; et al. *Gaussian 09*, Revision C.01; Gaussian: Wallingford, CT, USA, 2009.
(50) Heitz, S.; Weidauer, D.; Rosenow, B.; Hese, A. Measurement of Static Polarizabilities on $C_{10}H_8$ and $C_{10}D_8$. *J. Chem. Phys.* **1992**, *96*, 976−981.
(51) Stanton, J. F.; Gauss, J. The First Excited Singlet State of *s*-Tetrazine: A Theoretical Analysis of Some Outstanding Questions. *J. Chem. Phys.* **1996**, *104*, 9859−9869.
(52) Jansik, B.; Jonsson, D.; Salek, P.; Ågren, H. Calculations of Static and Dynamic Polarizabilities of Excited States by Means of Density Functional Theory. *J. Chem. Phys.* **2004**, *121*, 7595−7600.
(53) Foresman, J. B.; Head-Gordon, M.; Pople, J. A.; Frisch, M. J. Toward a Systematic Molecular Orbital Theory for Excited States. *J. Phys. Chem.* **1992**, *96*, 135−149.
(54) Rice, J. E.; Handy, N. C. The Calculation of Frequency-Dependent Polarizabilities as Pseudo-Energy Derivatives. *J. Chem. Phys.* **1991**, *94*, 4959−4971.
(55) Ingrosso, F. Ph.D. thesis, University of Pisa, Pisa, Italy, 2005.
(56) (a) Allen, M. P.; Tildesley, D. J. *Computer Simulation of Liquids*; Clarendon Press: Oxford, U.K., 1987; Chapters 3 and 5. (b) All simulations in this paper were carried out using the DL_POLY_-CLASSIC software package: http://www.ccp5.ac.uk/DL_POLY_CLASSIC. See: Todorov, I. T.; Smith, W.; Trachenko, K.; Dove, M. T. DL_POLY_3: New Dimensions in Molecular Dynamics Simulations via Massive Parallelism. *J. Mater. Chem.* **2006**, *16*, 1911−1918.
(57) Berendsen, H. J. C.; Postma, J. P. M.; van Gunsteren, W. F.; DiNola, A.; Haak, J. R. Molecular-Dynamics with Coupling to an External Bath. *J. Chem. Phys.* **1984**, *81*, 3684−3690.
(58) Ladanyi, B. M.; Stratt, R. M. Short-Time Dynamics of Solvation: Linear Solvation Theory for Polar Solvents. *J. Phys. Chem.* **1995**, *99*, 2502−2511.
(59) Passino, S.; Nagasawa, Y.; Joo, T.; Fleming, G. R. Three-Pulse Echo Peak Shift Studies of Polar Solvation Dynamics. *J. Phys. Chem. A* **1997**, *101*, 725−731.
(60) Ryu, S.; Stratt, R. M. A Case Study in the Molecular Interpretation of Optical Kerr Effect Spectra: Instantaneous-Normal-Mode Analysis of the OKE Spectrum of Liquid Benzene. *J. Phys. Chem. B* **2004**, *108*, 6782−6795.